International Journal of Refrigeration 133 (2022) 259–266

Contents lists available at ScienceDirect

International Journal of Refrigeration

journal homepage: www.elsevier.com/locate/ijrefrig

Common fault effects on a natural refrigerant, variable-speed heat pump

Effets des défaillances courantes sur une pompe à chaleur à vitesse variable fonctionnant avec un frigorigène naturel

I. Bellanco [a,b,*], F. Belío [a], M. Vallés [b], R. Gerber [c], J. Salom [a]

[a] Catalonia Institute for Energy Research (IREC), Jardins de les Dones de Negre 1, Sant Adrià del Besòs, Barcelona 08930, Spain
[b] Universitat Rovira i Virgili, Department of Mechanical Engineering, Av. Països Catalans No. 26, Tarragona 43007, Spain
[c] Heim AG Heizsysteme, Wittenwilerstrasse 31, Aadorf 8355, Switzerland

ARTICLE INFO

Keywords:
Fault detection and diagnosis
Variable refrigerant flow system
Failure analysis
Natural refrigerants

Mots clés:
Détection des défaillances et diagnostic
Système à débit de frigorigène variable
Analyse des défaillances
Frigorigènes naturels

ABSTRACT

The European heat pump market is growing every year as European legislation moves towards the use of natural refrigerants that have less global warming potential than conventional refrigerants. Even though heat pumps are very efficient, the appearance of hard-to-detect faults increases energy consumption. The present study emulated some of the most common faults on a variable-speed heat pump charged with propane. The faults tested were evaporator fouling, compressor valve leakage, liquid line restriction and refrigerant overcharge. The effect of these faults on performance and several heat pump features are described. Evaporator fouling was the fault with least COP degradation and compressor valve leakage with the most (7% and 56% COP reduction, respectively). The results are compared with the results from a comparable study. The heat pump covered the demand generated by nearly all the faults at the expense of increasing the power consumption. The features of each fault are summarized in a chart, which could be used as table for diagnosing faults.

1. Introduction

In the European Union, space heating, water heating and space cooling account for 79.2% of the energy consumption in households (Eurostat, 2021). Electricity is the main source of space cooling, whereas gas is the main source of space and water heating (Eurostat, 2021). Heat pumps are one of the most efficient technologies for space heating and cooling (Nowak, 2018) and, coupled with renewable electricity sources they can reduce greenhouse emissions released by heating. However, refrigerant leaks and incorrect disposal at the end of life can increase greenhouse emission. For this reason, the European Union is moving towards the use of natural refrigerants such as propane or carbon dioxide, which have a lower global warming potential (GWP) (Corberan 2016).

Despite their high performance, heat pumps could be working below their design efficiency (Domanski et al., 2014) because of incorrect system design and installation, and the appearance of faults that can remain undetected. These types of faults are known as soft faults because the equipment still covers the demand but energy consumption increases (Breuker and Braun, 1998). And they can turn into hard faults, which prevent the equipment from covering the load (Breuker and Braun, 1998) or even from working properly. Hard faults are usually detected by the user or by the maintenance services. However, soft faults can be undetected for long periods of time, thus increasing energy consumption and operating costs. Fault detection and diagnosis Fault detection and diagnosis (*FDD*) systems can be used to detect soft faults and monitor the efficiency of the equipment (Jagpal, 2006). These systems monitor several heat pump features to detect deviations from normal behavior (Katipamula and Brambley, 2005), determine which features are affected and diagnose the fault.

The effect of faults on fixed capacity heat pumps has been extensively studied for years (Breuker and Braun, 1998; Kim et al., 2006). However, the standard typology nowadays is the variable speed heat pump *VSHP* which can change the compressor speed to adapt to the demand. This feature helps to overcome the effects of faults, making it even more difficult to detect soft faults (Kim and Kim, 2005). Very little literature has been published on how common faults affect this type of heat pump. Noël et al. (2018) tested an air-to-water variable speed heat pump with

* Corresponding author at: Catalonia Institute for Energy Research (IREC), Jardins de les Dones de Negre 1, Sant Adrià del Besòs, Barcelona 08930, Spain
E-mail address: ibellanco@irec.cat (I. Bellanco).

https://doi.org/10.1016/j.ijrefrig.2021.10.017
Received 9 August 2021; Received in revised form 19 October 2021; Accepted 29 October 2021
Available online 3 November 2021

Table 1
Steady-state test conditions. From the water side: condenser outlet temperature ($T_{cond,out}$), condenser inlet temperature($T_{cond,in}$), evaporator inlet temperature ($T_{evap,in}$), condenser water flow ($\dot{V}_{cond}$) and evaporator water flow ($\dot{V}_{evap}$).

Heating load (kW)	$T_{cond,out}$ (°C)	$T_{cond,in}$ (°C)	$T_{evap,in}$ (°C)	$\dot{V}_{cond}$ (lpm)	$\dot{V}_{evap}$ (lpm)
10.2	45	40	10	30	40
12.3	45	39	10	30	40

under and over-charge of refrigerant and evaporator and condenser fouling. After describing the effects on the coefficient of performance *COP*, compressor frequency and the features of each fault, they concluded that the impact on the variables needs to be understood to differentiate the faults. Kim and Kim (2005) tested a variable-speed, brine-to-water heat pump in cooling mode with an open-type reciprocating compressor. They tested such faults as compressor valve leakage *CVL*, undercharge, and condenser and evaporator faults. The condenser and evaporator faults were emulated by reducing the transfer area of the heat exchangers and extracting the secondary fluid from several subsections of the heat exchangers. The results were compared with a fixed capacity heat pump, and it was found that the COP degradation was higher for the variable speed pump. They concluded that more experimental research should be done to find out how to operate *VSHP* with faults. Guo et al. (2017) tested refrigerant over and under-charge, a faulty four-way reversing valve and fouling of the outdoor heat exchanger on an air-to-water, variable-speed heat pump in heating mode. However, their paper focuses on the results of their data mining based FDD, and the fault effects are not shown. Li et al. (2018) tested the same equipment but in cooling conditions, and concluded that they needed more fault data to train their *FDD*. These articles show that the effects of faults in variable-speed heat pumps are different than in fixed speed pumps. The COP degradation is higher in *VSHP*. And they all conclude that more experimental studies need to be made on how faults affect VSHP, as this data could help to train and validate *FDD*.

The present study contributes to *FDD* research by adding new fault data for *VSHP*. Tests were made on a variable-speed water-to-water propane-charged heat pump without faults and with imposed common faults (Bellanco et al., 2021b). The faults emulated were evaporator fouling (*EF*), compressor valve leakage (*CVL*), liquid line restriction (*LL*) and refrigerant overcharge (*OC*). Different levels of fault intensity were applied with different heat duties, and the effects are described. The COP degradation between faults is compared, and the effects are summarized in a trend chart. The results could be used to train *FDD* algorithms and to distinguish between different faults to diagnose VSHP. This is the first study to be made of a variable speed heat pump charged with natural refrigerants.

The present study is structured as follows. We shall move on to Section 2, which describes the emulation of each fault. Then, in Section 3 the heat pump tested and the sensors used are described. Section 4 shows the results for the most affected features and describe the effects. Then, the effect of the faults on the COP is compared. In the discussion section, the results are compared with those of a previous study. A chart summarizes the trend of the features so that it can be used as a diagnosis chart. Finally, the conclusions describe the paper's key points with outlook for future research.

2. Methodology

For the current study, two steady-state conditions were tested: one with a load of 10.2 kW and the other with a load of 12.3 kW. The condenser supply temperature was set to 45 °C, and the return temperatures were set to 40 °C and 39 ° for the lower and higher load, respectively. The water flow was fixed. Table 1 shows the different setpoints on the demand and source side for the two conditions in which the faults EF, CVL, LL and OC were tested.

Table 2
EF steady-state tests experimental plan.

Code	Load (kW)	FI_{EF}
EF10.1	10.2	− 0.100
EF10.2	10.2	− 0.157
EF10.3	10.2	− 0.214
EF10.4	10.2	− 0.271
EF10.5	10.2	− 0.328
EF10.6	10.2	− 0.385
EF10.7	10.2	− 0.442
EF10.8	10.2	− 0.500
EF12.1	12.3	− 0.100
EF12.2	12.3	− 0.157
EF12.3	12.3	− 0.214
EF12.4	12.3	− 0.271
EF12.5	12.3	− 0.328
EF12.6	12.3	− 0.385
EF12.7	12.3	− 0.442
EF12.8	12.3	− 0.500

2.1. Evaporator fouling

Evaporator fouling (*EF*) represents a circulating pump malfunction or the accumulation of dirt in the circuit, which reduces the evaporator flow. The higher effect of this fault is the reduction of flow on the secondary fluid (air, water or brine) (Bellanco et al., 2021b). This fault is emulated by reducing the evaporator water flow to below the nominal value (Bellanco et al., 2021b). The indicator fault intensity (*FI*) is used to characterize each fault level (Yuill and Braun, 2013). The FI_{EF} is shown in Eq. (1).

$$FI_{EF} = \frac{\dot{V}_{fault} - \dot{V}_{nom}}{\dot{V}_{nom}} \quad (1)$$

where $\dot{V}_{fault}$ is the evaporator water flow for the current fault level and $\dot{V}_{nom}$ is the evaporator water flow for the no-fault condition. Table 2 shows the experimental plan followed for the steady-state tests.

2.2. Compressor valve leakage

The compressor valve leakage (*CVL*) fault represents the bypass of refrigerant between the high and low-pressure sides. This leakage can appear in the compressor or in the reversing valves (Bellanco et al., 2021b). A pipe that bypasses the suction and discharge lines of the compressor was installed to emulate the fault. A valve allows the line to be opened or closed.

The *FI* for this fault is shown in Eq. (2).

$$FI_{CVL} = \frac{\dot{m}_{r\_fault} - \dot{m}_{r\_nom}}{\dot{m}_{r\_nom}} \quad (2)$$

where $\dot{m}_{r\_fault}$ is the refrigerant mass flow for the fault condition, and $\dot{m}_{r\_nom}$ is the refrigerant mass flow when no fault is present. As the heat pump has a variable-speed compressor, $\dot{m}_{r\_nom}$ depends on the speed of the compressor. A correlation between compressor speed and refrigerant mass flow was obtained by running the compressor at different speeds without any faults, and measuring the refrigerant mass flow at steady state.

The experimental plan is shown in Table 3.

Table 3
CVL steady-state tests experimental plan.

Code	Load (kW)	FI_{CVL}
CVL10.1	10.2	− 0.042
CVL10.2	10.2	− 0.296
CVL10.3	10.2	− 0.372
CVL10.4	10.2	− 0.648
CVL12.1	12.3	− 0.131
CVL12.2	12.3	− 0.379
CVL12.3	12.3	− 0.608

Table 4
LL steady-state tests experimental plan.

Code	Load (kW)	FI_{LL}
LL10.1	10.2	0.103
LL10.2	10.2	0.181
LL10.3	10.2	0.267
LL10.4	10.2	0.418
LL10.5	10.2	0.743
LL12.1	12.3	0.055
LL12.2	12.3	0.168
LL12.3	12.3	0.281
LL12.4	12.3	0.404
LL12.5	12.3	0.648

Table 5
OC steady-state tests experimental plan.

Code	Load (kW)	FI_{OC}
OC10.1	10.2	0.1
OC12.1	12.3	0.1

2.3. Liquid line restriction

The liquid line restriction (*LL*) appears when the filter located in the liquid line is clogged. To emulate this fault, the manufacturer placed a restriction valve in the liquid line to increase the pressure drop (Bellanco et al., 2021b).

The *FI* of this fault is related to the pressure drop variation in the liquid line as Eq. (3) shows.

$$FI_{LL} = \frac{\Delta P_{LL} - \Delta P_{nom}}{\Delta P_{nom}} \tag{3}$$

where ΔP_{LL} represents the liquid line pressure drop with the fault and ΔP_{nom} the liquid line pressure drop without the fault. The pressure drop in the liquid line was calculated as the pressure difference between the discharge and suction lines.

The experimental plan is shown in Table 4.

2.4. Refrigerant overcharge

The refrigerant overcharge (*OC*) fault may appear during maintenance if the heat pump is filled with more refrigerant than recommended by the manufacturer. To emulate this fault, the heat pump was overcharged by 10% above the nominal amount. The FI_{OC} is the relative difference between the current and the nominal charge, as Eq. (4) shows.

$$FI_{OC} = \frac{m_{r\_fault} - m_{r\_nom}}{m_{r\_nom}} \tag{4}$$

where m_{r_fault} is the propane charge for faulty conditions, and m_{r_nom} is the nominal propane charge. Table 5 shows the experimental plan. An overcharge of 20% was also tested, but the heat pump could not run properly. As the heat pump has a small nominal charge (720 g), it may be more sensitive to variations in charge.

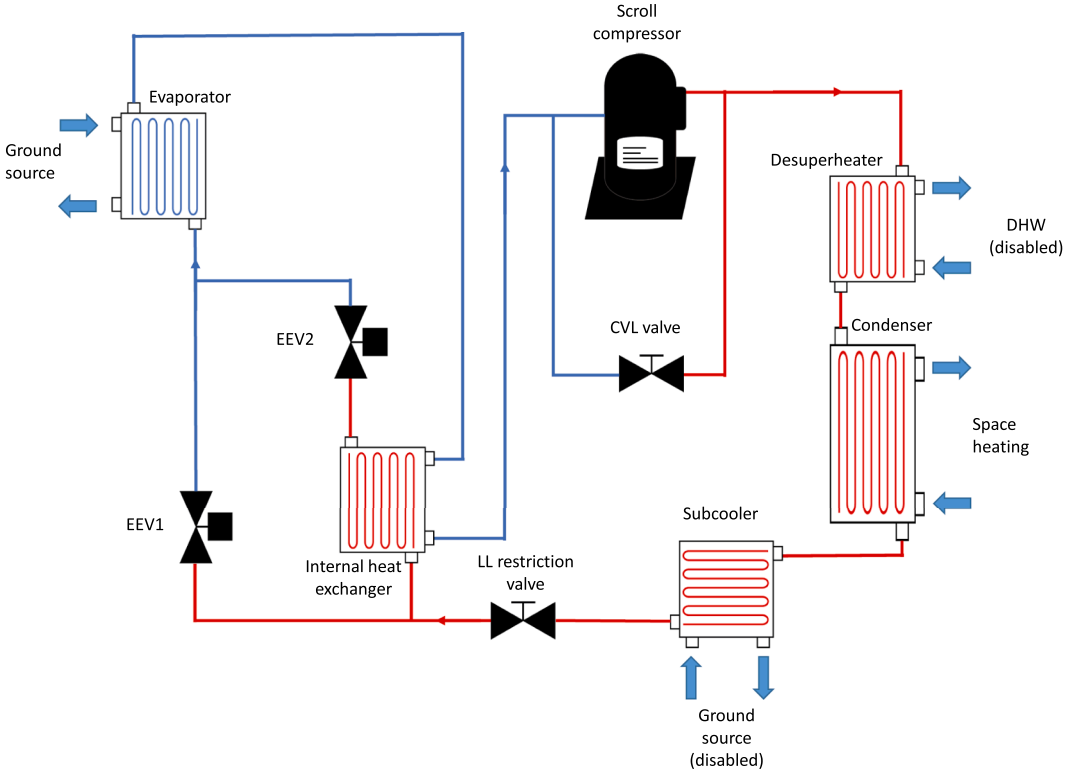

Fig. 1. Heat pump scheme. The desuperheater and subcooler were not used during the tests.

Table 6
Test measurements precision.

Magnitude	Type	Precision
Pressure	Piezo-resistive	± 1.00%
Refrigerant mass flow meter	Coriolis	± 0.10%
Temperature refrigerant liquid side	Pt1000	± 0.15 K
Temperature refrigerant gas side	NTC	± 0.30 K
Temperature water side	Pt100	± 0.25 K
Electrical power	Multimeter	± 1.00%
Water Flow	Electromagnetic	± 0.50%

3. Description of the tested heat pump

For the present study, a 10 kW, variable-speed water-to-water heat pump was tested. The heat pump used was a prototype charged with 720 g of propane as the refrigerant. Fig. 1 shows the heat pump architecture. The compressor used is a hermetic scroll type YHV0461U from Emerson. It is specifically designed for propane applications and to meet the requirements of flammable refrigerants. A Carel inverter type power+ was used to control the compressor. Both the condenser and evaporator are brazed plate heat exchangers in countercurrent arrangement. The desuperheater is used for domestic hot water (DHW) production. The internal heat exchanger used the heat from the condensed liquid to function as a suction gas superheater. Its capacity was controlled by a separate expansion valve. The prototype has internal pressure and temperature sensors and a Coriolis flowmeter for the refrigerant mass flow measurement. A compressor frequency setpoint can be sent to the heat pump but has no internal speed control. We developed a PID control that adapted the compressor frequency to the difference between the condenser water supply temperature and a setpoint.

The temperatures of the refrigerant circuit were obtained with NTC

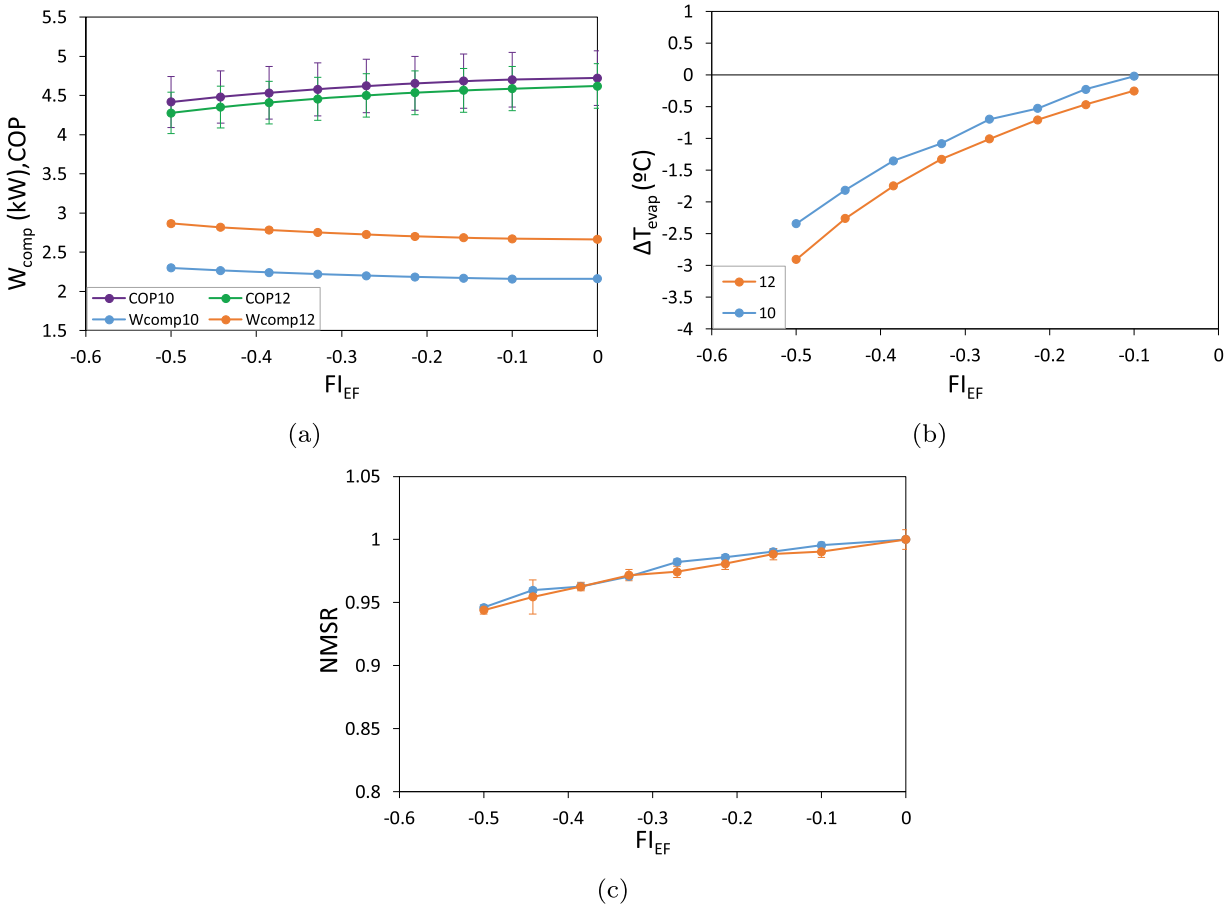

Fig. 2. Relevant features affected by the evaporator fouling fault (EF) for the 10 kW and 12 kW steady-state tests. Effect on: a) COP and compressor power consumption, b) evaporator saturation temperature and c) NMSR.

Table 7
Results for the overcharge test for 10 kW and 12 kW. FI: fault intensity, *COP*, W_{comp}: compressor electrical power consumption, Q_{heat}: condenser heating power, T_{sc}: subcooling, T_{sh}: superheating, T_{evap}: evaporator saturation temperature, T_{cond}: condenser saturation temperature, T_{co}: compressor outlet refrigerant temperature, T_{ll}: liquid line refrigerant temperature, $\dot{m}_r$: refrigerant mass flow, f: compressor speed.

Code	FI	COP	W_{comp} kW	Q_{heat} kW	T_{sc} K	T_{sh} K	T_{evap} °C	T_{cond} °C	T_{co} °C	T_{ll} °C	$\dot{m}_r$ g s^{-1}	f Hz
OC10.1	0.1	3.6	2.8	10.1	24.9	10.7	7.0	64.8	84.8	40.0	29	52
Uncertainty		±0.27	± 0.03	± 0.75	± 0.03	± 0.03	± 0.03	± 0.03	± 0.15	± 0.15	± 0.04	± 0.03
OC12.1	0.1	3.7	3.3	12.2	25.7	9.9	6.8	64.6	83.5	39.1	35	62
Uncertainty		±0.22	± 0.03	± 0.75	± 0.03	± 0.03	± 0.03	± 0.03	± 0.15	± 0.15	± 0.05	± 0.03

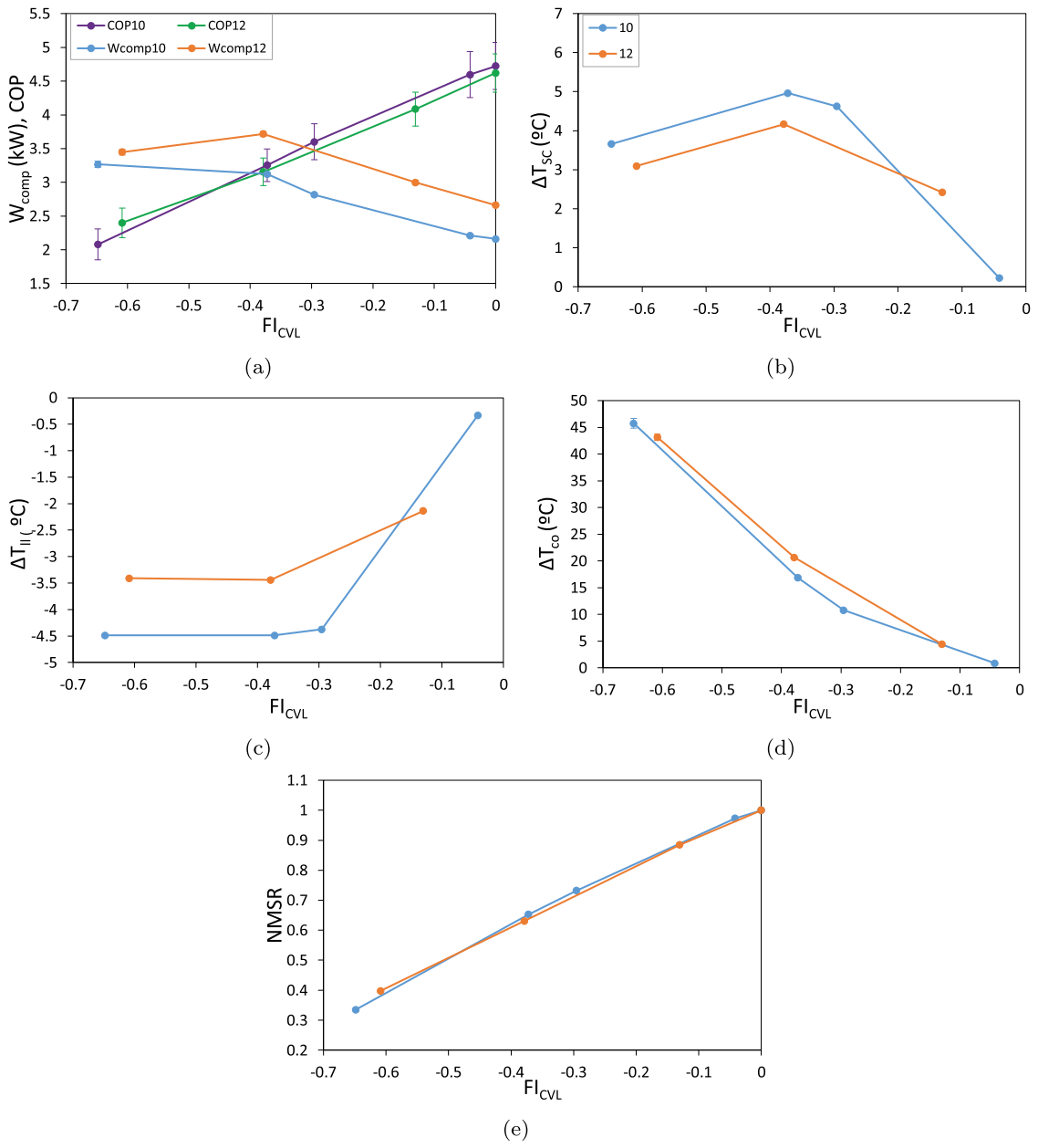

Fig. 3. Relevant features affected by the compressor valve leakage (CVL) fault for the 10 kW and 12 kW steady-state tests. Effect on: a) COP and compressor power consumption, b) subcooling, c) liquid line refrigerant temperature, d) compressor outlet refrigerant temperature and e) NMSR.

temperature probes at the suction line and with Pt1000 for the rest of the circuit. The duty was measured on the waterside with Pt100 probes and flowmeters. The pressure measurements were obtained with pressure transducers. The compressor speed was provided by the inverter and the power consumption was measured with a multimeter. Table 6 shows the precision of each sensor. The uncertainty of the tests were calculated using the Guide to Uncertainty in Measurement methods (JCGM, 2008). The dataset has been uploaded to the open-acces repository Zenodo (Bellanco et al., 2021a).

4. Results

Different heat pump features can be affected by each fault. The features selected for this study were the *COP*, compressor power consumption W_{comp}, condenser heat duty Q_{heat}, subcooling T_{sc}, superheating T_{sh}, evaporator saturation temperature T_{evap}, condenser saturation temperature T_{cond}, compressor outlet refrigerant temperature T_{co}, liquid line refrigerant temperature T_{ll}, refrigerant mass flow $\dot{m}_r$ and compressor speed f.

In a variable-speed heat pump, the refrigerant mass flow depends on the compressor speed and the inlet density, which in turn depends on the evaporation temperature. When a fault occurs, the heat pump may change the compressor speed to meet the new demand, changing the mass flow rate. Therefore, the refrigerant mass flow should be interpreted in terms of compressor speed. Because of this, the ratio between the refrigerant mass flow rate and the compressor speed (*MSR*) is used (Eq. (5)). The units are grams per revolution.

$$MSR = \frac{\dot{m}_r}{f} \tag{5}$$

Eq. (6) shows the normalized value of MSR (*NMSR*), which is more intuitive.

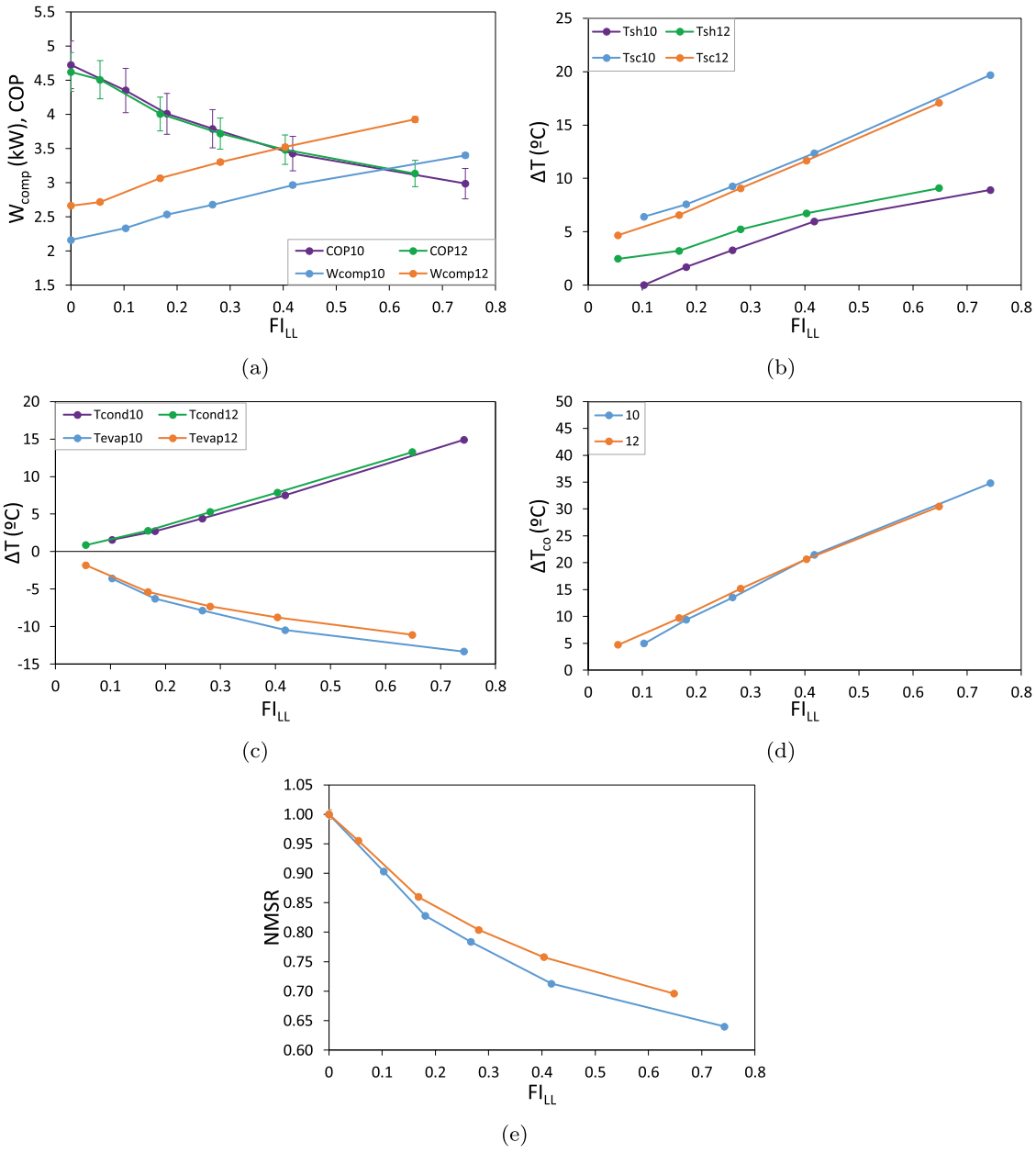

Fig. 4. Relevant features affected by the liquid line restriction (LL) fault for the 10 kW and 12 kW steady-state tests. Effect on: a) COP and compressor power consumption, b) superheating and subcooling, c) condenser saturation temperature and evaporator saturation temperature, d) compressor outlet refrigerant temperature and e) NMSR.

$$NMSR = \frac{MSR_{fault}}{MSR_{nominal}} \tag{6}$$

Figs. 2, 3 and 4 and Table 7 show the effects of the different faults. Only the features affected by each fault are shown. For T_{sc}, T_{sh}, T_{evap}, T_{cond}, T_{co} and T_{ll}, the difference between the no-fault value (T_{nom}) and the current level fault (T_{fault}) was used (see Eq. (7)). The ΔT for FI of 0, is 0.

$$\Delta T = T_{fault} - T_{nom} \tag{7}$$

For *EF*, reducing the water flow lowers the evaporator pressure, which decreases the evaporation temperature and increases the evaporator outlet temperature. The compressor speed increases so that demand can still be covered, which decreases NMSR and increases power consumption.

The *CVL* fault increases the pressure at the suction line while the discharge pressure remains the same. To compensate for all the refrigerant that goes through the bypass, the compressor increases the speed, which increases the power consumption and the compressor outlet temperature. This increase in the outlet temperature triggers a safety limitation of the compressor speed. This limitation causes a decrease in power consumption at the highest fault level, as Fig. 3a shows. At that fault level, the refrigerant mass in the circuit is so low that the demand can not be covered. The outlet temperature increases, forcing the compressor to stop for its safety.

The *LL* causes an additional pressure loss between condensation pressure and suction pressure. With low restriction values, the two expansion valves open simultaneously and there is no effect on the COP or other variables. When the restriction increase, the main valve (EEV1) is fully open, superheat at the evaporator outlet increases while the other valve (EEV2) closes. This reduces the refrigerant liquid line temperature by 4.5 °C and 3.5 °C for the lower and the higher load, respectively. Since the first FI value, the EEV1 reaches its capacity limit, and the refrigerant starts to be retained in the condenser leading to more

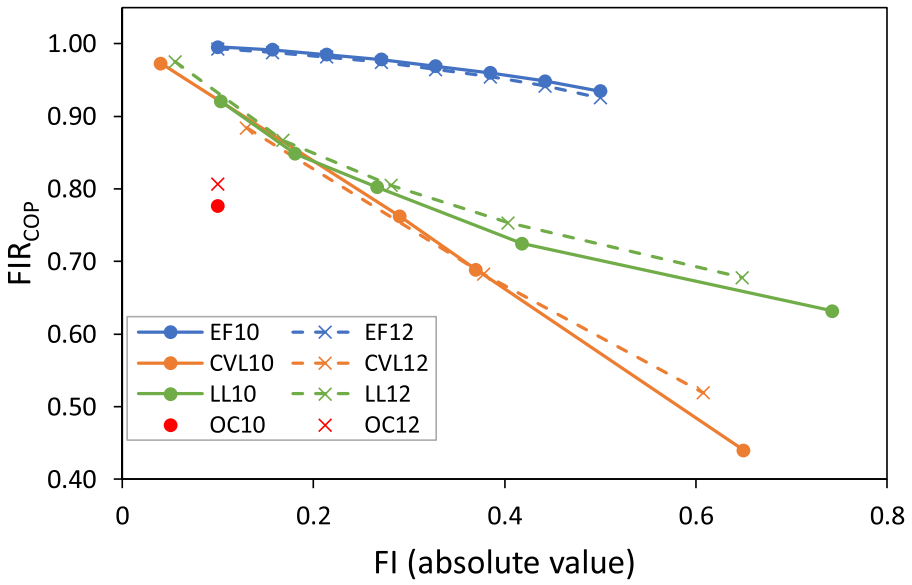

Fig. 5. Fault impact ratio on the COP for each fault intensity. The fault intensity is shown in absolute value.

subcooling. Because there is liquid trapped in the condenser, the temperature of the refrigerant at the outlet of the condenser approaches the temperature at the inlet of the water side, therefore the T_{ll} values are constant for all the fault levels. The condensation temperature increases while the evaporation temperature decreases. The compressor speed increases to cover the demand, which decreases the NMSR and increases the power consumption.

The *OC* fault increases the liquid trapped in the condenser, which increases the condensation temperature. The evaporation temperature increases due to an increase in suction pressure. The subcooling and the compressor outlet temperatures rise. The refrigerant mass flow rate slightly increases while the speed of the compressor drops, which increases the NMSR. This fault has little or no effect on systems with a liquid receiver (Kim and Kim, 2005).

Table 8
Trend for each of the features for the present study and the study by Kim and Kim (2005).↑: increasing trend, ↓: decreasing trend.

Fault	COP	T_{sc}	T_{co}	f
EF	↓		↑	↑
EF_Kim	↓		↑	↑
CVL	↓	↑	↑	↑
CVL_Kim	↓		↑	↑

5. Discussion

The fault impact ratio on COP (FIR_{COP}) is used to compare the extent to which each fault degrades COP (Yuill and Braun, 2013). Eq. (8) shows how it is calculated. A FIR_{COP} of one indicates that the COP does not change.

$$FIR_{COP} = \frac{COP_{fault}}{COP_{nominal}} \tag{8}$$

Fig. 5 shows the FIR_{COP} for each fault. All the faults decreased the *COP* of the heat pump, with EF having the least effect and CVL the most. As the heat duty is usually not affected, the decrease in COP comes from an increase in electrical power consumption. The heat duty remains the same for all the faults except at the highest value of CVL. There are no significant differences between the results with different loads.

The study that is most similar to ours, is the paper by Kim and Kim (2005), which uses a brine-to-water heat pump, but in cooling mode. They tested the faults CVL, OC, EF (in their case, the ground source heat exchanger is the condenser), undercharge and condenser fouling. They have measurements from the water and brine circuits, but also have the features T_{cond}, T_{sc}, T_{co}, and f. Table 8 compares the results of these two studies. For CVL, Kim found an increase in the compressor speed and outlet temperature, but the FI stayed 0.2, which may explain the lack of effect on other features. At the same fault level, we also found an increase in T_{sc}. For EF, it is difficult to compare the two systems because Kim worked in cooling mode. However, COP was affected more severely

Table 9
Trend for each of the features. ↑↑: high increasing trend, ↑: increasing trend, ↓: decreasing trend, ↓↓: high decreasing trend. The last two rows describe the criteria applied for constructing the table.

Fault	COP	W_{comp}	Q_{heat}	T_{sc}	T_{sh}	T_{evap}	T_{cond}	T_{co}	T_{ll}	$\dot{m}_r$	f	MSR
EF	↓	↑				↓					↑	
CVL	↓↓	↑↑	↓↓	↑				↑↑	↓	↓↓	↑↑	↓↓
LL	↓↓	↑↑		↑↑	↑↑	↓↓	↑↑	↑↑	↓	↓↓	↑↑	↓↓
OC	↓	↑↑		↑↑		↑	↑↑	↑↑	↓		↓	↑
↑↑,↓↓	± 1	± 0.5 kW	± 1 kW	± 5 °C	± 5 °C	± 5 °C	± 5 °C	± 5 °C	± 5 °C	± 5 g s^{-1}	± 15 Hz	± 15 g r^{-1}
↑, ↓	± 0.1	± 0.1 kW	± 0.2 kW	± 2 °C	± 2 °C	± 2 °C	± 2 °C	± 2 °C	± 2 °C	± 2 g s^{-1}	± 3 Hz	± 3 g r^{-1}

in their case than in ours. The OC had no effect on the COP in their system due to a liquid receiver. In general, it is difficult to make a direct comparison between both systems. The heat pump in Kim's study had a liquid line receiver which could change the effects of the faults as in the case of OC (Hu et al., 2021).

Table 9 summarizes the feature trends for each fault of the propane heat pump and the results help to develop a diagnosis system. For example, an *FDD* could be developed by training no-fault models for each feature. Once these models have been trained, the model results are compared with the real measurements and, depending on the trends, the fault can be diagnosed (Rogers et al., 2019). For example, if the T_{sh} trend increases, the fault diagnosed will be LL. Obtaining more experimental results on *VSHP* helps to improve the *FDD* solutions and develop new ones.

6. Conclusions

Some of the common faults for heat pumps have been emulated in a variable-speed water-to-water heat pump in heating mode. The heat pump was a prototype charged with propane, which aligns with the legislation on the use of refrigerants with lower *GWP*. The tests showed:

- EF had little impact on the heat pump, although it halve the water flow.
- CVL had an impact on subcooling and the liquid line temperature. It considerably increased the compressor outlet temperature and the speed of the compressor.
- LL had an impact on nearly all the features studied.
- OC affected nearly all features except superheating, which remained constant because of the electronic expansion valves *EEV*.
- All the faults decreased the COP. EF was the fault with the least effect and CVL the one with the most.
- The demand could not be covered only at the highest value of CVL. For all the other faults, the heat pump increased the compressor speed to cover the demand, which increased the electrical power consumption. This situation could go unnoticed by the user because the demand is still covered.

The comparison of the results with a similar study shows equivalent trends. However, the different working modes (heating or cooling) and different internal components (presence of liquid line receiver) hinder the direct comparison. A chart with the trends of the different features has been provided. This chart could be used to validate a diagnose system based on trend comparison, but it could be limited to this specific heat pump. Further work includes testing the FDD developed with dynamic and field conditions.

Declaration of Competing Interest

The authors declare that they have no known competing financial interests or personal relationships that could have appeared to influence the work reported in this paper.

Acknowledgments

Ivan Bellanco acknowledges the Universities and Research Secretariat of the Catalan Government and the European Social Fund for the financial support of the predoctoral contract 2019FI_B 00928. The research conducted in this paper is partially funded by the European Unions Horizon 2020 research and innovation program under grant agreement no. 814888 (TRI-HP).

References

Bellanco, I., Belío, F., Gerber, R., Salom, J., 2021a. Common faults tested on a variable-speed propane-charged heat pump on heating mode. 10.5281/zenodo.5155136.

Bellanco, I., Fuentes, E., Vallès, M., Salom, J., 2021. A review of the fault behavior of heat pumps and measurements, detection and diagnosis methods including virtual sensors. J. Build. Eng. 39 (August 2020) https://doi.org/10.1016/j.jobe.2021.102254.

Breuker, M.S., Braun, J.E., 1998. Common faults and their impacts for rooftop air conditioners. HVAC&R Res. 4 (3), 303–318. https://doi.org/10.1080/10789669.1998.10391406.

Corberan, J.M., 2016. New Trends and Developments in Ground-Source Heat Pumps. Elsevier Ltd. https://doi.org/10.1016/B978-0-08-100311-4.00013-3.

Domanski, P.A., Henderson, H.I., Payne, W.V., Domanski, P.A., Henderson, H.I., Payne, W.V., 2014. Sensitivity Analysis of Installation Faults on Heat Pump Performance. Technical report.

Eurostat. Energy consumption in households. Accessed: 2021-04-09. https://ec.europa.eu/eurostat/statistics-explained/index.php?title=Energy_consumption_in_households#Energy_consumption_in_households_by_type_of_end-use.

Guo, Y., Li, G., Chen, H., Wang, J., Guo, M., Sun, S., Hu, W., 2017. Optimized neural network-based fault diagnosis strategy for VRF system in heating mode using data mining. Appl. Therm. Eng. 125, 1402–1413. https://doi.org/10.1016/j.applthermaleng.2017.07.065.

Hu, Y., Yuill, D.P., Ebrahimifakhar, A., Rooholghodos, A., 2021. An experimental study of the behavior of a high efficiency residential heat pump in cooling mode with common installation faults imposed. Appl. Therm. Eng. 184 (September 2020), 116116. https://doi.org/10.1016/j.applthermaleng.2020.116116.

Jagpal, R., 2006. Technical Synthesis Report IEA Annex 34: Computer Aided Evaluation of HVAC System Performance. Technical report.

J. C. f. G. on Metrology, 2008. Evaluation of Measurement Data - Guide to the Expression of Uncertainty in Measurement. Technical report September. http://www.bipm.org/en/publications/guides/gum.html.

Katipamula, S., Brambley, M.R., 2005. Review article: methods for fault detection, diagnostics, and prognostics for building systems a review, part I. HVAC&R Res. 11 (1) https://doi.org/10.1080/10789669.2005.10391133.

Kim, M., Kim, M.S., 2005. Performance investigation of a variable speed vapor compression system for fault detection and diagnosis. Int. J. Refrig. 28 (4), 481–488. https://doi.org/10.1016/j.ijrefrig.2004.11.008.

Kim, M., Payne, W.V., Domanski, P.A., Yoon, S.H., Hermes, C.J., 2006. Performance of a residential heat pump operating in the cooling mode with single faults imposed. Appl. Therm. Eng. 29 (4), 770–778. https://doi.org/10.1016/j.applthermaleng.2008.04.009.

Li, G., Chen, H., Hu, Y., Wang, J., Guo, Y., Liu, J., Li, H., Huang, R., Lv, H., Li, J., 2018. An improved decision tree-based fault diagnosis method for practical variable refrigerant flow system using virtual sensor-based fault indicators. Appl. Therm. Eng. 129, 1292–1303. https://doi.org/10.1016/j.applthermaleng.2017.10.013.

Noël, D., Teuillières, C., Rivière, P., Cauret, O., Marchio, D., 2018. Experimental Characterization of Fault Impacts on the Functioning Variables of an Inverter Driven Heat Pump(January 2019).

Nowak, T., 2018. Heat Pumps: Integrating Technologies to Decarbonise Heating and Cooling. Technical report.

Rogers, A.P., Guo, F., Rasmussen, B.P., 2019. A review of fault detection and diagnosis methods for residential air conditioning systems. Build. Environ. 161 (July), 106236. https://doi.org/10.1016/j.buildenv.2019.106236.

Yuill, D.P., Braun, J.E., 2013. Evaluating the performance of fault detection and diagnostics protocols applied to air-cooled unitary air-conditioning equipment. HVAC&R Res. 19 (7), 882–891. https://doi.org/10.1080/10789669.2013.808135.